

Seismic traveltimes inversion of 3D velocity model with triangulated interfaces

Fei Li · Tao Xu · Minghui Zhang · Zhenbo Wu · Chenglong Wu · Zhongjie Zhang · Jiwen Teng

Received: 2 September 2013 / Accepted: 29 September 2013 / Published online: 30 November 2013

© The Seismological Society of China, Institute of Geophysics, China Earthquake Administration, and Springer-Verlag Berlin Heidelberg 2013

Abstract Seismic traveltimes tomographic inversion has played an important role in detecting the internal structure of the solid earth. We use a set of blocks to approximate geologically complex media that cannot be well described by layered models or cells. The geological body is described as an aggregate of arbitrarily shaped blocks, which are separated by triangulated interfaces. We can describe the media as homogenous or heterogeneous in each block. We define the velocities at the given rectangle grid points for each block, and the heterogeneous velocities in each block can be calculated by a linear interpolation algorithm. The parameters of the velocity grid positions are independent of the model parameterization, which is advantageous in the joint inversion of the velocities and the node depths of an interface. We implement a segmentally iterative ray tracer to calculate traveltimes in the 3D heterogeneous block models. The damped least squares method is employed in seismic traveltimes inversion, which includes the partial derivatives of traveltimes with respect to the depths of nodes in the triangulated interfaces and velocities defined in rectangular grids. The numerical tests indicate that the node depths of a triangulated interface and homogeneous velocity distributions can be well inverted in a stratified model.

Keywords Traveltimes inversion · 3D · Triangulated interface · Block modeling

1 Introduction

Since Aki and Lee (1976) first brought the technology of medical CT to the area of seismology to image the velocity structure of the crust and upper mantle, seismic tomography has become one of the most important ways to detect the internal structure of the solid earth. Seismic tomography is a technique of imaging 3D seismic velocity and/or attenuation structure of the earth by combining information from a large number of crisscrossing seismic waves triggered by natural energy sources (earthquakes) or artificial sources (explosions and vibroseis) (Zhao 2001). The obtained high-resolution tomographic models of the earth have provided constraints on the global tectonic processes, lithosphere evolution and deformation, the rule and dynamic mechanism of plate movement, differences in the deep structure between continents and oceans, and the existence of heterogeneous structures in volcanic areas, earthquake faults, subduction zones, and other diverse geological environments (Zhao 2001; Tian et al. 2009). According to the data used, seismic tomography can be divided into body wave tomography and surface wave tomography. The lateral resolution of body wave tomography is relatively higher, but the vertical resolution is highly variable due to the nearly vertical incoming ray. Nowadays, the most commonly used method is still body wave (especially P wave) traveltimes tomography among all the methods of seismic tomography. The parameters to be inverted have already been broadened from velocity inversion to velocity and hypocentral location inversion or velocity and interface depth inversion simultaneously (e.g.,

Zhongjie Zhang (1964–2013)

F. Li (✉) · T. Xu · M. Zhang · Z. Wu · C. Wu · Z. Zhang · J. Teng

State Key Laboratory of Lithospheric Evolution, Institute of Geology and Geophysics, Chinese Academy of Sciences, Beijing 100029, China
e-mail: lifei@mail.iggcas.ac.cn

F. Li · M. Zhang · Z. Wu · C. Wu
University of Chinese Academy of Sciences, Beijing 100049, China

Aki and Lee 1976; Aki et al. 1977; Pavlis and Booker 1980; Liu 1984; Zhao et al. 1992; Bishop et al. 1985; Zelt and Smith 1992; Hua and Liu 1995; Rawlinson et al. 2001; Zhou et al. 2006; Huang and Bai 2010; Bai et al. 2011). Zhao (2001) and Rawlinson et al. (2010) had made systematic summaries about the development and achievement of seismic tomography at different periods.

Seismic traveltime tomography is based on model parameterization and the associated forward ray tracing methods to calculate the traveltimes. The solid earth can be described as a continuous or discrete medium, of which the discrete one is often parameterized in grids (or cells) (Vidale 1988, 1990; Moser 1991). The frequently used grid parameterization is rectangular grid (cubic in 3D) with velocities defined at the grid nodes. The discrete models have a good adjustability and the corresponding traveltime calculation and ray tracing are robust, e.g., eikonal equation and its solver for calculating the traveltimes (Vidale 1988, 1990; Lan and Zhang 2013a, b), and shortest path ray tracing (e.g., Moser 1991; Zhao et al. 2004) and so on. A fine grid-based model can be a good approximation to reality, while the major challenges lie in: firstly, it is hard to describe complex models with fine structures, especially when describing continuously fluctuant tectonic interfaces with discrete grid nodes, sometimes the interfaces need to be redefined; secondly, a huge number of grid nodes are needed in describing complex geologic structures, and the memory space and tracing time increase dramatically with a reduced node spacing and the growth of the node number for accuracy purposes. Accordingly, the model parameterization in grids is dramatically dependent on the memory space and calculating speed of the computer, especially in the 3D case.

A commonly used method to describe continuous medium is model parameterization in layers. In some situations, a horizontally layered model is fairly efficient in describing geologic structures and very convenient for ray tracing (e.g., Zelt and Smith 1992; Zhang et al. 2003, 2005, 2013; Zhang and Klemperer 2005; Zhang and Wang 2007). It becomes quite difficult for layered parameterization in the case of complex 3D geologic models such as reverse fault, and hence layered models are inapplicable for some cases in realistic seismic exploration. A block model can faithfully represent such complex structures as faults, pinch-out layers, intrusive tectonics, and lens, whereas model parameterization and corresponding ray tracing are more complex (Xu et al. 2004, 2006, 2008, 2010; Li et al. 2013). In block model parameterization, a geologic model is regarded as an aggregate of arbitrarily shaped blocks. Gjystdal et al. (1985) first used a block modeling technique to generate 3D models, and the geologic blocks were described in a manner similar to the set operation, which was not that intuitionistic. Pereyra (1996) developed the technique of block modeling, and the describing of the

blocks became more intuitionistic and spontaneous; however, the interfaces of the models were described with B-spline, which confined the geologic models to such typical structure as pinch-out or intrusive tectonics. In this paper, we follow describing the geologic models as an aggregate of arbitrarily shaped blocks separated by triangulated interfaces, theoretically geologic models with arbitrary complex structures can be parameterized in this way (Xu et al. 2004, 2006, 2008, 2010; Li et al. 2013).

Traditional kinematic ray tracing methods include shooting (Virieux and Farra 1991; Sun 1993; Sambridge et al. 1995; Xu et al. 2004, 2008) and bending (Julian and Gubbins 1977; Thurber and Ellsworth 1980; Pereyra et al. 1980; Keller and Perozzi 1983; Um and Thurber 1987; Prothero et al. 1988; Pereyra 1992; Xu et al. 2006, 2010; Li et al. 2013). Shooting methods are at an advantage in the global search for the receivers, while bending methods have a relatively higher tracing efficiency. Other reported ray tracing methods include wavefront techniques (Vinje et al. 1993, 1996), shortest path ray tracing (Moser 1991; Zhao et al. 2004; Zhang et al. 2000), and simulated annealing (Velis and Ulrych 1996, 2001). The methods mentioned above have the advantage of tracing for the global minimum traveltime ray paths. Cervený (2001) made a good summary of these methods. In our previous work, we have implemented a robust segmentally iterative ray tracer (SIRT) for fast ray tracing in complex block media, which has a good adaptability in 3D media with a constant velocity (Xu et al. 2006) or a constant gradient velocity distribution (Xu et al. 2010). Recently, we have developed the block models to more complex heterogeneous media with arbitrary velocity distributions defined in the blocks, and developed the SIRT to adapt to the new heterogeneous models. Combining SIRT with pseudo-bending method (Um and Thurber 1987), we proposed a three-point perturbation scheme for fast ray tracing in complex heterogeneous models (Li et al. 2013). In this paper, based on the block model and fast and robust SIRT method in 3D complex media, we develop the body wave traveltime inversion of the velocities and the node depths of an interface. The damped least squares method is employed in the seismic traveltime inversion.

2 Model parameterization

2.1 3D block models with triangulated interfaces

In block model parameterization, we describe a geologic model as an aggregate of arbitrarily shaped blocks separated by triangulated interfaces. The blocks are endowed with different geologic attributes (e.g., seismic wave velocity, density etc.), and the neighboring blocks share the

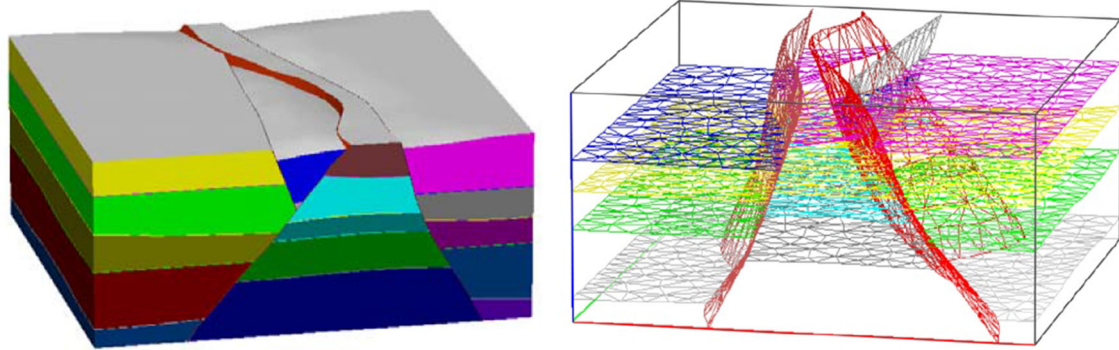


Fig. 1 The horst structure model is described as an aggregate of blocks; different blocks are shown in different colors (left) and separated by triangulated interfaces (right)

same interface (Xu et al. 2004, 2006). The structure of the 2D media is represented hierarchically as area → element → edge → point (Xu et al. 2010). Geologic elements are closed regions separated by edges, which are cubic splines interpolated by discrete points. The structure of the 3D media is represented hierarchically as volume → block → interface → triangle → point (Xu et al. 2004, 2006, 2008, 2010; Li et al. 2013). The interfaces between different blocks are pieced together by a series of triangulated surface patches.

In this paper, we represent the triangulated interfaces in the same way as our previous works (Xu et al. 2004, 2006, 2008, 2010; Li et al. 2013). Compared with Coons, Bezier, B-spline, triangulated interface has a lot of advantages. Triangulated interfaces are also applied in the well-known GOCAD system (Mallet 1989, 1992). For more detailed advantages and disadvantages of block models with triangulated interfaces, see Xu et al. (2006) and Li et al. (2013). Normal vectors hold constants inside a triangle and vary abruptly across the linked boundary of two triangles that are not in the same plane. As a result, a reflected or transmitted ray may change direction abruptly across linked boundaries. To avoid this difficulty, we have introduced an algorithm to redefine normal vectors at arbitrary points on an interface so that normal vectors are continuous on the whole interface (Xu et al. 2004, 2006, 2008, 2010; Li et al. 2013). Figure 1 gives a complex 3D block model with triangulated interfaces, the model contains 18 blocks, 6,676 triangles, and 2,700 discrete points. The model is designed for representing the features of the graben-horst structure in an extensional basin. This kind of structure is widespread within the basins in the eastern China, such as the Bohai Sea, Subei and Songliao basins, China.

2.2 Heterogeneous velocity distribution in a block

We can describe the media as homogenous or heterogeneous in each block. To describe the heterogeneous

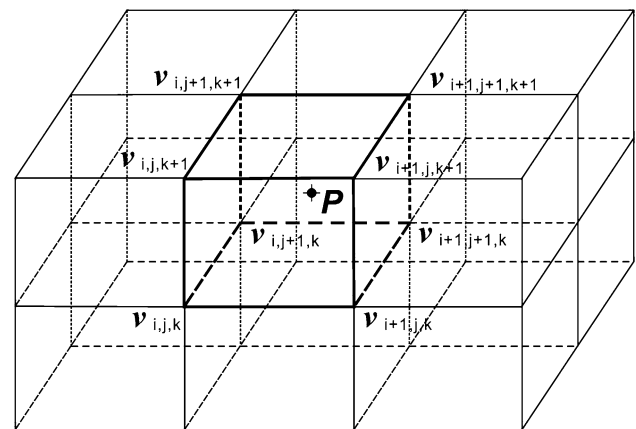


Fig. 2 Heterogeneous velocity distribution is to define a set of discrete velocity nodes. A trilinear interpolation function is used to describe the velocity at point P within a rectangular grid of nodes

velocity distribution in 3D block models, the velocity distribution in each block of the geologic model is redefined all alone. We define the velocities at the given cubic grid points for each block, and thus the heterogeneous velocity at any position in each block can be calculated by a linear interpolation algorithm. As shown in Fig. 2, for a certain point $P(x, y, z)$ in a 3D block model, first we should find its location in the cubic mesh, and then the velocity $v(x, y, z)$ at point P , can be calculated by a trilinear interpolation of the velocities at the surrounding cubic grid points as follows:

$$v(x, y, z) = \sum_{l=0}^1 \sum_{m=0}^1 \sum_{n=0}^1 v(i+l, j+m, k+n) \left(1 - \left| \frac{x-x_{i+l}}{x_{i+1}-x_i} \right| \right) \times \left(1 - \left| \frac{y-y_{j+m}}{y_{j+1}-y_j} \right| \right) \left(1 - \left| \frac{z-z_{k+n}}{z_{k+1}-z_k} \right| \right), \tag{1}$$

where $v(i+l, j+m, k+n)$ denotes velocity at the cubic grid points, x_i, y_j, z_k denotes x, y, z coordinates of cubic grid points, respectively.

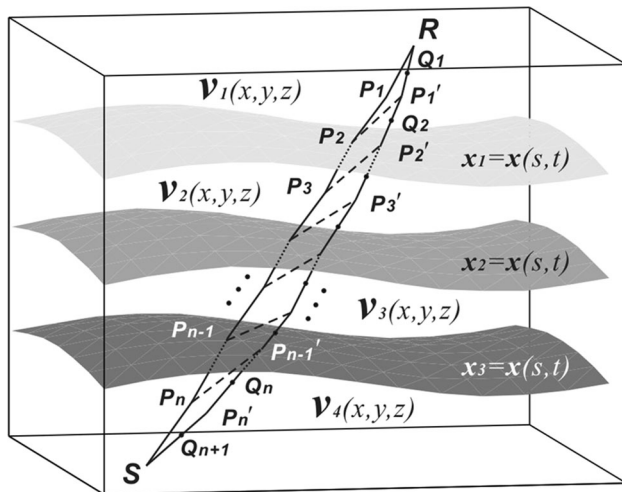


Fig. 3 The sketch of the ray tracing scheme of combination of segmentally iterative methods and pseudo-bending methods

3 Ray tracing in 3D heterogeneous block models

Um and Thurber (1987) proposed a pseudo-bending method for two-point ray tracing in continuous media. Pseudo-bending can only be applied to continuous velocity distributions, and it fails to work when velocity discontinuities exist. We have proposed a SIRT to calculate traveltimes in the 3D models with velocity discontinuities. SIRT has a good adaptability in 3D media with a constant velocity (Xu et al. 2006), a constant gradient velocity distribution (Xu et al. 2010), and a heterogeneous velocity distribution (Li et al. 2013).

A successive three-point perturbation scheme is formulated that iteratively updates the midpoints of a segment based on an initial ray path. The corrections of the midpoints are accomplished by first-order analytic formulae according to the locations of the midpoints inside the blocks (e.g., points P_1 , P_3 and P_n in Fig. 3) or on the boundaries of the blocks (e.g., points P_2 and P_{n-1} in Fig. 3), to which the updating formulae of the pseudo-bending method and SIRT algorithm are applied instead of the traditional iterative methods (Li et al. 2013).

Figure 4 shows the ray tracing results in a 3D combination model (Fig. 4a) with heterogeneous velocity distributions in different blocks. The model, with a size of $5 \times 5 \times 5$ km, has 7 blocks, 4,649 triangles, 2,152 points, and is composed of normal faults, reverse faults, an intrusive mass, and a lens. A vertical cross section (X - Z) at position $y = 2.5$ km of the heterogeneous velocity distribution is given in Fig. 4b. The shot (\star in Fig. 4b) is located at the position of (4.35, 2.5 km) on the surface, 207 receivers are arranged in a 23×9 rectangle. The upper

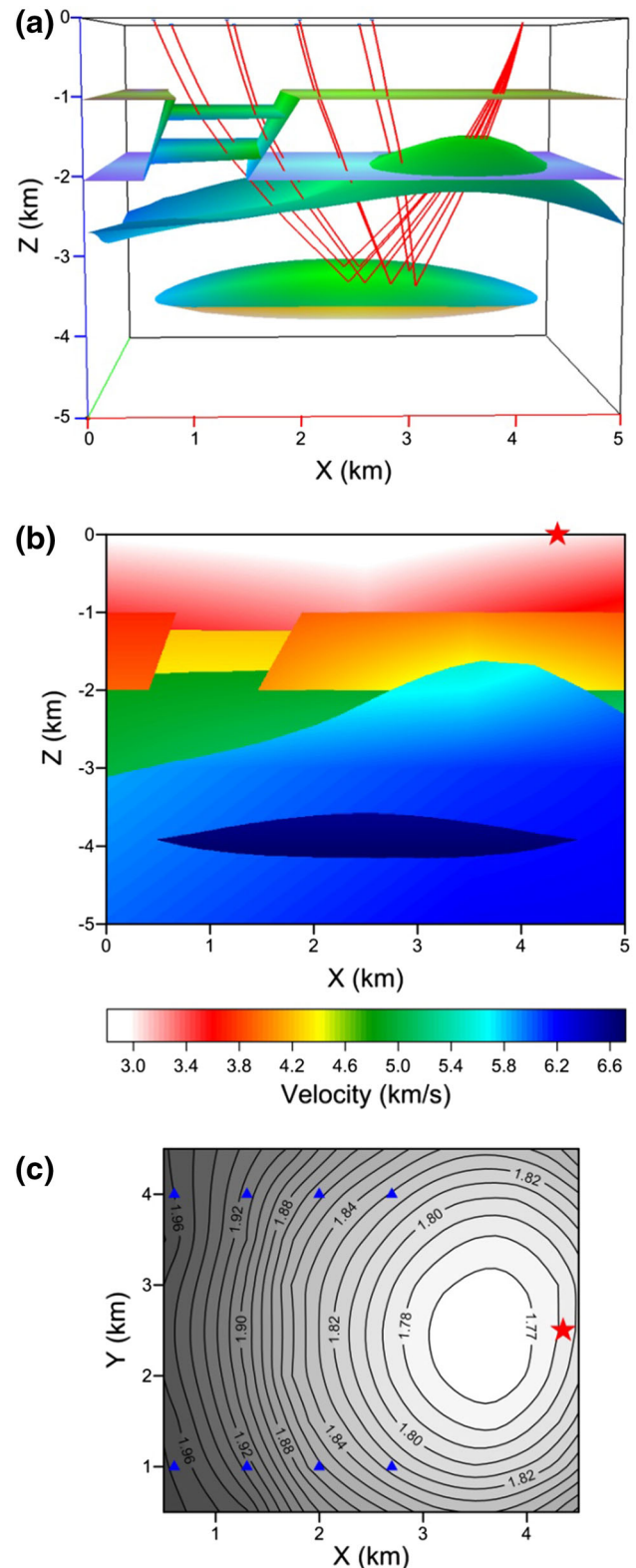


Fig. 4 a 3D ray tracing results in the combination model with heterogeneous velocity distributions in different blocks. b Velocity slice at the position $y = 2.5$ km. c Associated traveltimes isolines

interface of the lens is defined as the reflecting interface. Note that only eight ray paths are selected for a clear display. The associated traveltimes against the x- and y-coordinates is shown in Fig. 4c.

4 Traveltime inversion procedure

4.1 Damped least squares method

All the tomographic problems finally lead to an observation equation that relates the data to the source and medium parameters (Zhao 2001)

$$d = Gm + e, \tag{2}$$

where d, m, e are vectors for data, unknown parameters and errors, respectively. G is the coefficient matrix, whose elements consist of the partial derivatives of traveltimes with respect to hypocentral and velocity parameters. A single row of the matrix G consists of the derivatives of the traveltimes for a particular ray with respect to each of the parameters in the model. In this paper, the elements of G are the partial derivatives of traveltimes with respect to the depths of nodes in the triangulated interfaces and velocities defined in rectangular grids. In many circumstances, the inversion of model parameters can be regarded as linearly according to the damped least squares principle (Aki and Lee 1976; Aki et al. 1977; Zelt and Smith 1992).

The vector for model parameters changes in the damped least squares inversion can be expressed as

$$\Delta m = (G^T G + \alpha I)^{-1} G^T \Delta T, \tag{3}$$

where Δm is the model parameter adjustment vector, which can be the changes of the velocities or interface depths; I is a unit vector, α is a damping factor; $\Delta T = T_{\text{obs}} - T_{\text{cal}}$ is the traveltimes residual vector; the partial derivative matrix G is the same as in Eq. (2). The introduction of damping factor α can not only ensure the stability of the matrix inversion, but also keep the model parameter adjustment vector Δm not that large during each iterative process. The value of α is determined by the practical models.

4.2 Partial derivatives matrix

4.2.1 Velocity partial derivatives of traveltimes

The traveltimes T between a source S and receiver R along a ray path is given in integral form for a continuous

velocity field $v(x, y, z)$ in 3D heterogeneous block models as

$$T = \int_S^R \frac{1}{v(x, y, z)} dl, \tag{4}$$

where $v(x, y, z)$ denotes the velocity distribution at any point in the model, which can be calculated from formula (1), dl is the integral unit along a ray path. As described above, we combine SIRT with pseudo-bending and put forward a successive three-point perturbation scheme for ray tracing in complex 3D heterogeneous media with velocity discontinuities (Li et al. 2013), and the ray path should be a series of continuous ray path segments, thus we can have an approximate discrete form of formula (4):

$$T = \sum_{k=1}^n \frac{l_k}{2} \left(\frac{1}{v_{k,s}} + \frac{1}{v_{k,e}} \right), \tag{5}$$

where l_k is the path length of the k th ray segment, $v_{k,s}$ and $v_{k,e}$ are velocities at the start point and end point of the k th ray segment, respectively, n is the number of the ray segments along a ray path.

Because the heterogeneous velocities at any position of each block are calculated by a trilinear interpolation of the velocities at the surrounding cubic grid points, so the velocities at the cubic grid points become the velocity parameters selected for inversion. From formula (5), we can get the partial derivatives of traveltimes with respect to the velocities defined at the cubic grid points:

$$\frac{\partial T}{\partial v_m} = \sum_{k=1}^n -\frac{l_k}{2} \left(\frac{1}{v_{k,s}^2} \frac{\partial v_{k,s}}{\partial v_m} + \frac{1}{v_{k,e}^2} \frac{\partial v_{k,e}}{\partial v_m} \right), \tag{6}$$

where v_m denotes the velocity at the m th cubic grid point selected for inversion; $v_{k,s}$ and $v_{k,e}$ are the velocities at the start point and end point of the k th ray segment along the ray path, respectively; $\frac{\partial v_{k,s}}{\partial v_m}$ and $\frac{\partial v_{k,e}}{\partial v_m}$ are the partial derivatives of $v_{k,s}(x, y, z)$ and $v_{k,e}(x, y, z)$ with respect to v_m , respectively, which can be calculated from formula (1); T, l_k, n and k are the same as in the formulas above. The values of the partial derivatives $\frac{\partial v_{k,s}}{\partial v_m}$ and $\frac{\partial v_{k,e}}{\partial v_m}$ in formula (6) are equal to zero except when a ray segment is located inside some cubic grid containing the grid point selected for inversion, because in this case the ray path and traveltimes are changed with the change of v_m . Suppose a typical point of a ray path segment is surrounded by eight grid points, then the integral values of the partial

derivatives β_k (e.g., $\frac{\partial v_k}{\partial v_m}$) in Eq. (6) are equal to zero except on these eight points,

normal vector perpendicular to the plane triangle $A_{j-1}A_jA_{j+1}$, then

$$\beta_k = \beta_k(u, v, w) = \begin{cases} \left(1 - \frac{|x - x_{u_0+l}|}{|x_{u_0+1} - x_{u_0}|}\right) \left(1 - \frac{|y - y_{v_0+m}|}{|y_{v_0+1} - y_{v_0}|}\right) \left(1 - \frac{|z - z_{w_0+n}|}{|z_{w_0+1} - z_{w_0}|}\right), \\ \text{if } u = u_0 + l, v = v_0 + m, w = w_0 + n, \\ 0, \text{ else} \end{cases} \tag{7}$$

where $l = 0, 1; m = 0, 1; n = 0, 1$.

4.2.2 Depth partial derivatives of travelttime

Similarly, the uplift or descent of the fluctuation interfaces in 3D block models can be achieved by changing the positions of the triangle vertexes, so the positions of the triangle vertexes become the interface parameters selected for inversion. For simplicity, the x - and y -coordinate of the interface triangle vertexes are fixed, only z -coordinate is a variable to be considered during inversion. The basic approach of calculating the Fréchet derivative is to partition the problem (Bishop et al. 1985; Nowack and Lyslo 1989; Zelt and Smith 1992; Rawlinson et al. 2001):

$$\frac{\partial T_i}{\partial z_j} = \frac{dT_i}{dh_{\text{int}}} \frac{dh_{\text{int}}}{dz_{\text{int}}} \frac{\partial z_{\text{int}}}{\partial z_j}, \tag{8}$$

where z_j is the depth coordinate of the interface node, h_{int} is the displacement normal to the interface at the point of intersection by the ray, and z_{int} is the depth coordinate of the intersection point.

From Fig. 5a, we can obtain the travelttime difference before and after the interface is changed,

$$\Delta T = \frac{OP'_k}{v_2} - \frac{OP_k}{v_1} \tag{9}$$

and since

$$OP'_k = -\mathbf{W}_{k+1} \cdot \mathbf{W}_n \Delta h_j, \quad OP_k = -\mathbf{W}_k \cdot \mathbf{W}_n \Delta h_j. \tag{10}$$

Note that all vectors are unit vectors, then

$$\Delta T = \left(\frac{\mathbf{W}_k \cdot \mathbf{W}_n}{v_1} - \frac{\mathbf{W}_{k+1} \cdot \mathbf{W}_n}{v_2} \right) \Delta h_j \tag{11}$$

and the partial derivative approximation is:

$$\frac{\partial T}{\partial h_{\text{int}}} \approx \frac{\mathbf{W}_k \cdot \mathbf{W}_n}{v_1} - \frac{\mathbf{W}_{k+1} \cdot \mathbf{W}_n}{v_2}. \tag{12}$$

Because the normal vector \mathbf{W}_n at point P_k is redefined according to a certain principle (Xu et al. 2006), which does not coincide with vector \mathbf{W}_t certainly, which is the

$$\frac{\partial h_{\text{int}}}{\partial z_{\text{int}}} = \frac{P_k N}{P_k M} = \frac{\mathbf{W}_t \cdot \mathbf{W}_z}{\mathbf{W}_t \cdot \mathbf{W}_n}. \tag{13}$$

If the area coordinate u_l ($l = 0, 1, 2$) denotes the position of point P_k in the triangle $A_{j-1}A_jA_{j+1}$ (Xu et al. 2006), then

$$\frac{\partial z_{\text{int}}}{\partial z_j} = \frac{P_k M}{\Delta z_j} = \frac{P_k Q}{A_j Q} = u_l, \tag{14}$$

where subscript l is the index of point P_k in the triangle $A_{j-1}A_jA_{j+1}$, e.g., A_j is the second order of three points A_{j-1}, A_j, A_{j+1} , which indicates $l = 1$ in this circumstance. Substitution of three partial derivatives into formula (8) gives

$$\frac{\partial T_i}{\partial z_j} = \left(\frac{\mathbf{W}_k \cdot \mathbf{W}_n}{v_1} - \frac{\mathbf{W}_{k+1} \cdot \mathbf{W}_n}{v_2} \right) \frac{\mathbf{W}_t \cdot \mathbf{W}_z}{\mathbf{W}_t \cdot \mathbf{W}_n} u_l. \tag{15}$$

Formula (15) is the ultimate expression of partial derivatives of travelttime with respect to the depths of nodes in the triangulated interfaces.

5 Synthetic model tests

We present several typical model tests using synthetic data to test our inversion methods. The observed travelttime here we use is approximated by adding random noise to calculated theoretic travelttime through ray tracing in 3D models with known velocity distribution and interface parameters for simplicity. These models, which are contained within cubes, are all composed of several blocks separated by triangulated interfaces.

5.1 Velocity inversion of 3D homogeneous model with fluctuant interfaces

Figure 6a shows a stratified model with two fluctuant interfaces underground. The model (model 1) has dimensions of $5 \times 5 \times 5$ km and is composed of 3 blocks and 180 triangles. The velocities in the first and second layer of

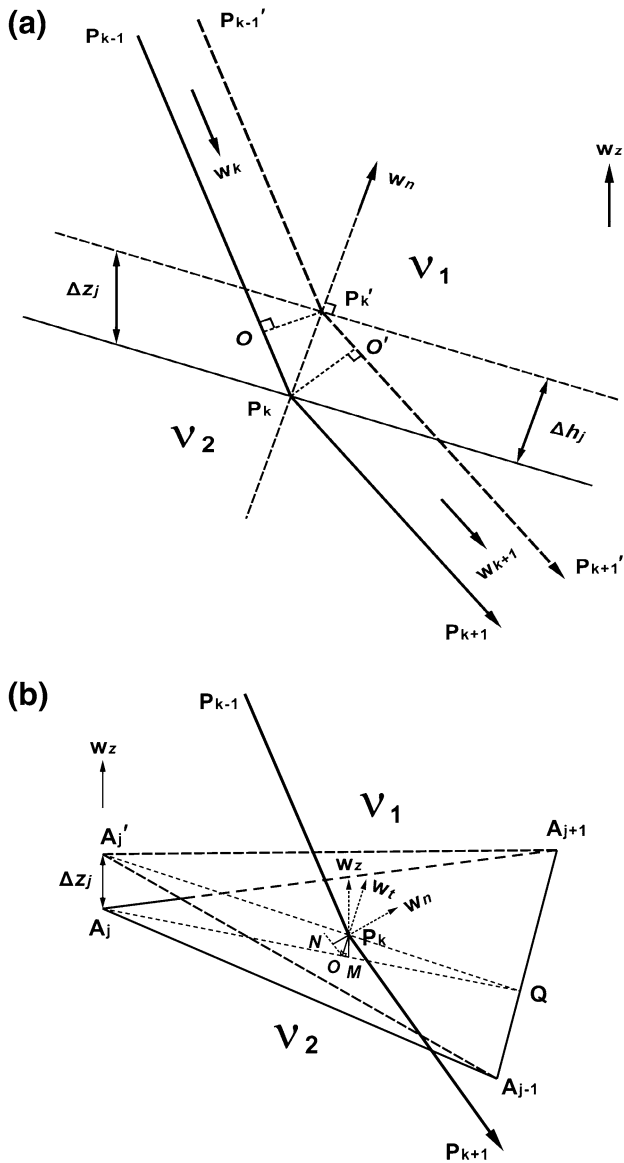


Fig. 5 Illustration of calculation of depth partial derivative

model 1 are defined as v_1 and v_2 , respectively. The source–receiver pairs designed for model 1 are also shown in Fig. 6a. The source–receiver pairs are located on the surface and the source is in the center of the surface of the model. Around the source 100 receivers are arranged in a 10×10 rectangle. In our tests, the second interface underground is defined as the reflecting interface. The incident rays are drawn in blue lines and the reflected rays are drawn in red lines. Only the reflected rays on the second interface are taken into consideration in our model test.

Figure 6b, c show the velocity inversion results of model 1. The true velocities in the first and second layer of model 1 are $v_1 = 4.8$ km/s and $v_2 = 5.4$ km/s, which are represented by green solid lines in Fig. 6b, c. In the

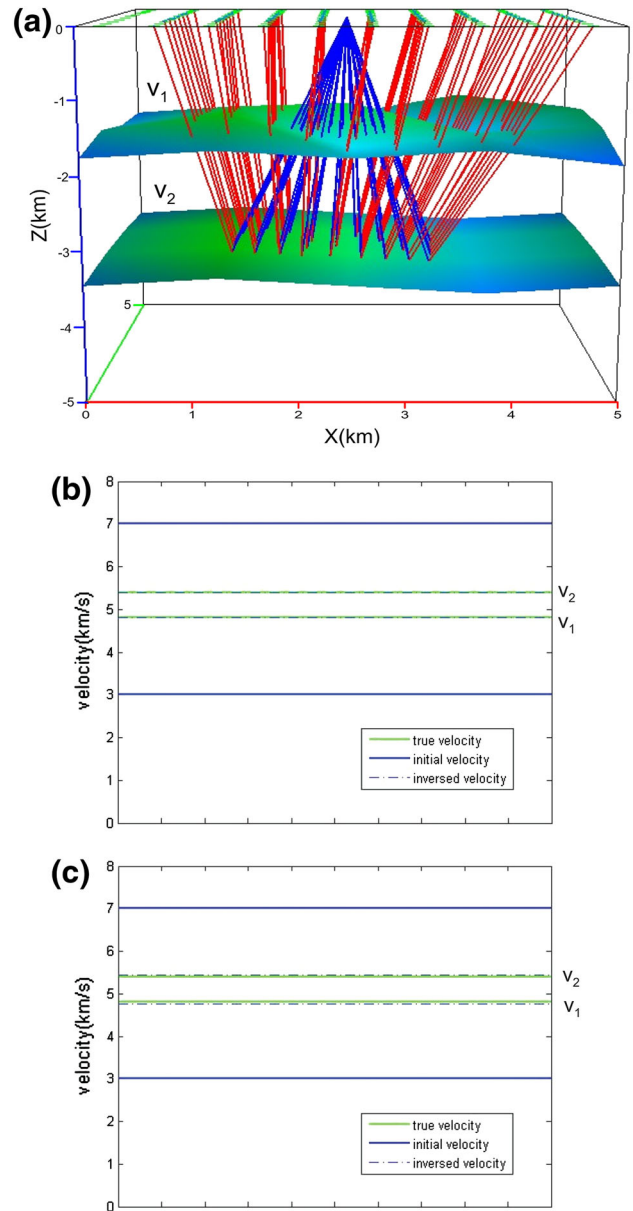


Fig. 6 Velocity inversion of 3D model with fluctuant interfaces. a Model 1 and the source–receiver pairs. b The result of velocity inversion with theoretic traveltimes after 5 iterations of the damped least squares method. c The result of velocity inversion with a maximum of 20 ms random noise added to the theoretic traveltimes

inversion procedure, the initial velocity of v_1 and v_2 are defined as 3.0 and 7.0 km/s, respectively, which are represented by blue solid lines in Fig. 6b, c. Figure 6b shows the result of velocity inversion with the input of theoretic traveltime after 5 iterations, and Fig. 6c shows the result of velocity inversion with the input of disturbed arrival times. From Fig. 6b, we can see that the velocity distribution can be well inverted by the theoretic traveltime even with initial velocity violently departs from the true velocity. The inverted velocities in Fig. 6c have some departure from the

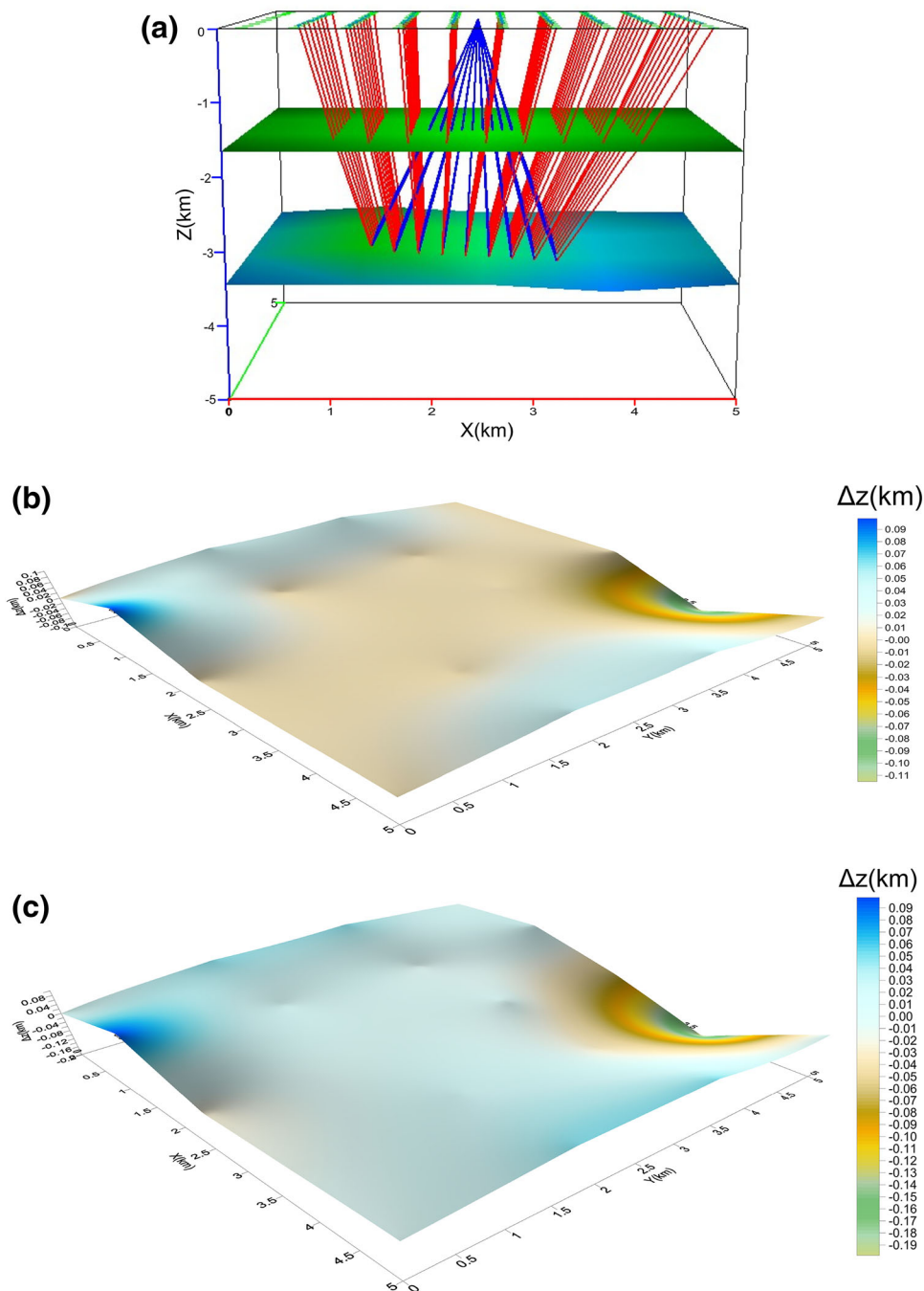


Fig. 7 Fluctuant interface geometry inversion of 3D model with triangulated interfaces. **a** Model 2 and the source–receiver pairs. **b** The fine difference between the true and inverted depths of the second fluctuant interface underground with theoretic traveltimes. **c** The fine difference between the true and inverted depths of the second fluctuant interface underground with a maximum of 10 ms random noise added to the theoretic traveltimes

true velocities of the model for the input of a maximum of 20 ms random noise added to the theoretic traveltimes. The inverted velocities which are represented by blue dotted lines in Fig. 6b, c can be obtained after 5 iterations of the damped least squares method.

5.2 Interface geometry inversion of 3D model with triangulated interfaces

Figure 7 shows the fluctuant interface geometry inversion of 3D model with triangulated interfaces. This model

(model 2) with dimensions of $5 \times 5 \times 5$ km also has the same source–receiver pairs as model 1 in Fig. 6. In model 2, the first interface underground is flat while the second one underground is fluctuant. In the inversion procedure, the position of the first interface underground is fixed and the depths of the triangular vertexes on the second fluctuant interface underground are to be inverted. The second interface is initialed as a flat one before the inversion, and we can obtain the fine differences between the true and inverted depths of the second fluctuant interface underground after several iterations. Figure 7b shows the fine differences between the true and inverted depths with the input of theoretic traveltimes after 5 iterations, and Fig. 7c shows the fine differences between the true and inverted depths with the input of a maximum of 10 ms random noise added to the theoretic traveltimes. From Fig. 7b, c, we can easily find that the interface geometry near the center of the second interface is better inverted compared with the several points near the edges of the interface. The relatively large error between the true and inverted depths of the several points near the edges of the fluctuant interface can be attributed to the lower ray coverage.

6 Conclusions

Block modeling combined with triangulated interfaces is efficient in 3D complex heterogeneous model building. The parameters of the velocity grid positions are independent of the model parameterization, which has been proved to be advantageous in the inversion of the velocities and the node depths of an interface. A successive three-point perturbation scheme of SIRT is used as a forward ray tracer for the traveltimes inversion of 3D velocity model with triangulated interfaces. The damped least squares method is employed in seismic traveltimes inversion, which includes the partial derivatives of traveltimes with respect to the depths of nodes in the triangulated interfaces and velocities defined in rectangular grids. Model tests using synthetic data indicate the fundamental validity of our velocity inversion of 3D homogeneous stratified model with fluctuant interfaces, as well as fluctuant interface geometry inversion of 3D model with triangulated interfaces. Simultaneous inversion of heterogeneous velocity distributions and fluctuant interface geometry is further considered in future.

Acknowledgments This study was supported financially by the Ministry of Science and Technology of China (2011CB808904), the National Natural Science Foundation of China (Nos. 41021063, 41174075, 41004034, 41174043, and 41274090). We are especially thankful to Drs. Xi Zhang, Haiqiang Lan and Minling Wang for their

constructive comments and suggestions to improve the quality of this work.

References

- Aki K, Lee WHK (1976) Determination of three dimensional velocity anomalies under a seismic array using first P arrival times from local earthquakes. *J Geophys Res* 81:4381–4399
- Aki K, Christofferson A, Husebye ES (1977) Determination of the three dimensional seismic structure of the lithosphere. *J Geophys Res* 82:277–296
- Bai CY, Huang GJ, Li ZS (2011) Simultaneous inversion combining multiple-phase travel times within 3D complex layered media. *Chin J Geophys* 54(1):182–192 (in Chinese with English abstract)
- Bishop TN, Bube KP, Cutler RT, Cutler RT, Langan RT, Love PL, Resnick JR, Shuey RT, Spindler DA, Wyld HW (1985) Tomography determination of the velocity and depth in laterally varying media. *Geophysics* 50:903–923
- Cerveny V (2001) *Seismic ray theory*. Cambridge University Press, New York
- Gjøystdal H, Reinhardsen JE, Åstebol K (1985) Computer representation of complex 3-D geological structures using a new “solid modeling” technique. *Geophys Prospect* 33:195–211
- Hua BL, Liu FT (1995) Joint reflection image of velocity and interface: theory and method. *Chin J Geophys* 38(6):750–756 (in Chinese with English abstract)
- Huang GJ, Bai CY (2010) Simultaneous inversion with multiple traveltimes with 2-D complex layered media. *Chin J Geophys* 53(12):2972–2981 (in Chinese with English abstract)
- Julian BR, Gubbins D (1977) Three-dimensional seismic ray tracing. *J Geophys* 43:95–113
- Keller HB, Perozzi DJ (1983) Fast seismic ray tracing. *SIAM J Appl Math* 43:981–992
- Lan H, Zhang Z (2013a) Topography-dependent eikonal equation and its solver for calculation first-arrival traveltimes with an irregular surface. *Geophys J Int* 193:1010–1026
- Lan H, Zhang Z (2013b) A high-order fast-sweeping scheme for calculating first-arrival travel times with an irregular surface. *Bull Seismol Soc Am* 103(3):2070–2082
- Li F, Xu T, Wu ZB, Zhang ZJ, Teng JW (2013) Segmentally iterative ray tracing in 3-D heterogeneous geological models. *Chin J Geophys* 56(10):3514–3522 (in Chinese with English abstract)
- Liu FT (1984) Simultaneous inversion of earthquake hypocenters and velocity structure(I): theory and method. *Chin J Geophys* 27(2):167–175 (in Chinese with English abstract)
- Mallet JL (1989) Discrete smooth interpolation. *ACM Trans Graphics* 8:121–144
- Mallet JL (1992) Discrete smooth interpolation in geometric modeling. *Comput Aided Des* 24:178–193
- Moser TJ (1991) Shortest path calculation of seismic rays. *Geophysics* 56:59–67
- Nowack RL, Lyslo JA (1989) Fréchet derivatives for curved interfaces in the ray approximation. *Geophys J* 97:497–509
- Pavlis LG, Booker JR (1980) The mixed discrete-continuous inverse problem: application to the simultaneous determination of earthquake hypocenters and velocity structure. *J Geophys Res* 85:4801–4810
- Pereyra V (1992) Two-point ray tracing in general 3-D media. *Geophys Prospect* 40:267–287
- Pereyra (1996) Modeling, ray tracing, and block nonlinear travel-time inversion in 3-D. *Pure Appl Geophys* 148:345–386

- Pereyra V, Lee WHK, Keller HB (1980) Solving two-point seismic-ray tracing problems in heterogeneous medium. Part 1. A general adaptive finite difference method. *Bull Seismol Soc Am* 70:79–99
- Prothero W, Taylor W, Eickemeyer (1988) A fast two-point, three-dimensional raytracing algorithm using a simple step search method. *Bull Seismol Soc Am* 78:1190–1198
- Rawlinson NG, Houseman A, Collins CDN (2001) Inversion of seismic refraction and wide-angle reflection traveltimes for three-dimensional layered crustal structure. *Geophys J Int* 145:381–400
- Rawlinson N, Pozgay S, Fishwick S (2010) Seismic tomography: a window into deep Earth. *Phys Earth Planet Inter* 178:101–135
- Sambridge M, Braun J, McQueen H (1995) Geophysical parameterization and interpolation of irregular data using natural neighbors. *Geophys J Int* 122:837–857
- Sun Y (1993) Ray tracing in 3-D media by parameterized shooting. *Geophys J Int* 114:145–155
- Thurber C, Ellsworth W (1980) Rapid solution of ray tracing problems in heterogeneous media. *Bull Seismol Soc Am* 70:1137–1148
- Tian Y, Zhao DP, Liu C, Teng JW (2009) A review of body-wave tomography and its applications to studying the crust and mantle structure in China. *Earth Sci Front* 16(2):347–360 (in Chinese with English abstract)
- Um J, Thurber C (1987) A fast algorithm for two-point seismic ray tracing. *Bull Seismol Soc Am* 77:972–986
- Velis DR, Ulrych TJ (1996) Simulated annealing two-point ray tracing. *Geophys Res Lett* 23:201–204
- Velis DR, Ulrych TJ (2001) Simulated annealing ray tracing in complex three-dimensional media. *Geophys J Int* 145:447–459
- Vidale JE (1988) Finite-difference calculation of travel times. *Bull Seismol Soc Am* 78:2062–2076
- Vidale JE (1990) Finite-difference calculations of traveltimes in three dimensions. *Geophysics* 55:521–526
- Vinje V, Iverson E, Gjøystdal H (1993) Traveltime and amplitude estimation using wavefront construction. *Geophysics* 58:1157–1166
- Vinje V, Iverson E, Astebol K, Gjøystdal H (1996) Estimation of multivalued arrivals in 3D models using wavefront construction. *Geophys Prospect* 44:819–842
- Virieux J, Farra V (1991) Ray tracing in 3-D complex isotropic media: an analysis of the problem. *Geophysics* 56:2057–2069
- Xu T, Xu GM, Gao EG, Zhu LB, Jiang XY (2004) Block modeling and shooting ray tracing in complex 3-D media. *Chin J Geophys* 47(6):1118–1126 (in Chinese with English abstract)
- Xu T, Xu GM, Gao EG, Li YC, Jiang XY, Luo KY (2006) Block modeling and segmentally iterative ray tracing in complex 3D media. *Geophysics* 71:T41–T51
- Xu T, Zhang Z, Zhao A, Zhang A, Zhang X, Zhang H (2008) Sub-triangle shooting ray tracing in complex 3D VTI media. *J Seism Explor* 17:131–144
- Xu T, Zhang ZJ, Gao EG, Xu GM, Sun L (2010) Segmentally iterative ray tracing in complex 2D and 3D heterogeneous block models. *Bull Seismol Soc Am* 100(2):841–850
- Zelt CA, Smith RB (1992) Seismic traveltime inversion for 2-D crustal velocity structure. *Geophys J Int* 108:16–34
- Zhang Z, Klemperer S (2005) West-east variation in crustal thickness in northern Lhasa block, central Tibet, from deep seismic sounding data. *J Geophys Res* 110:1–14
- Zhang Z, Wang Y (2007) Crustal structure and contact relationship revealed from deep seismic sounding data in South China. *Phys Earth Planet Inter* 165:114–126
- Zhang Z, Wang G, Teng J, Klemperer S (2000) CDP mapping to obtain the fine structure of the crust and upper mantle from seismic sounding data: an example for the southeastern China. *Phys Earth Planet Inter* 122:133–146
- Zhang Z, Lin G, Chen J, Harris JM, Han L (2003) Inversion for elliptically anisotropic velocity using VSP reflection traveltimes. *Geophys Prospect* 51:159–166
- Zhang Z, Badal J, Li Y, Chen Y, Yang L, Teng J (2005) Crust-upper mantle seismic velocity structure across Southeastern China. *Tectonophysics* 395:137–157
- Zhang ZJ, Xu T, Zhao B, Badal J (2013) Systematic variations in seismic velocity and reflection in the crust of Cathaysia: new constraints on intraplate orogeny in the South China continent. *Gondwana Res*. doi:10.1016/j.gr.2012.05.18
- Zhao D (2001) New advances of seismic tomography and its applications to subduction zones and earthquake fault zones: a review. *Island Arc* 10:68–84
- Zhao D, Hasegawa A, Horiuchi S (1992) Tomographic imaging of P and S wave velocity structure beneath northeastern Japan. *J Geophys Res* 97:19909–19928
- Zhao A, Zhang Z, Teng J (2004) Minimum travel time tree algorithm for seismic ray tracing: improvement in efficiency. *J Geophys Eng* 1(4):245–251
- Zhou LQ, Liu FT, Chen XF (2006) Simultaneous tomography of 3-D velocity structure and interface. *Chin J Geophys* 49(4):1062–1067 (in Chinese with English abstract)